iJRASET
International Journal For Research in Applied Science and Engineering Technology

INTERNATIONAL JOURNAL FOR RESEARCH

IN APPLIED SCIENCE & ENGINEERING TECHNOLOGY

Volume: 6 **Issue:** XII **Month of publication:** December 2018

DOI:

www.ijraset.com

Call: 08813907089 | E-mail ID: ijraset@gmail.com

International Journal for Research in Applied Science & Engineering Technology (IJRASET)
ISSN: 2321-9653; IC Value: 45.98; SJ Impact Factor: 6.887
Volume 6 Issue XII, Dec 2018- Available at www.ijraset.com

A Vibrational and DFT Study of (R)-( )-2 Pyrrolidinemethanol

Piyush Gupta[1], Rahul Tripathi[2], C. K Dixit[3], Sanjeev Kumar Trivedi[4]
[1]*North East Frontier Technical University, Arunachal Pradesh-791001*
[2, 3]*D.S.M.N.R. University, Lucknow -226017*
[4]*Mumtaz P.G College, Lucknow University, Lucknow-226020*

Abstract: ***Experimental IR and solution phase spectra of (R)-( )-2-Pyrrolidinemethanol showing evidence of hydro-gen bonding have been interpreted by computing vibrational modes of monomers and dimers with the molecular species due to intra- and inter-molecular hydrogen bonding, at B3LYP/6-311+G(d,p) level density functional theoretical calculations. Computed vibrational frequencies of Boltzmann population-weighted dimers for stretching and bending of OAH and NAH modes associated with the inter-molecular NAH O and OAH O hydrogen bonding are in good agreement with the measured IR absorption, Raman and solution-phase IR values near 3289 cm [1], 3450 cm [1] and 1400–1300 cm [1]. Further, the H O length is shorter in OAH O than in NAH O by 10% suggesting that OAH O is a stronger bond. While the solution-phase IR spectral features suggest strong inter-molecular associations, it is short of demonstrating which type of bonding is dominant factor. We conclude that the measured IR, Raman and solution-phase IR spectral features indicate the presence of both types of hydrogen bonds***

Keywords: DFT, Vibrational Analysis, FTIR, Molecular Orbital, Electronic Parameter, Thermodynamic parameter.

I. INTRODUCTION

Chiral molecules with optical activity and enantiomer-specific properties are increasingly used in drug discovery [1]. They also act as reagent intermediates in asymmetric synthesis of other chirals [2]. The (R)-( )-2-Pyrrolidinemethanol (2-PRDM, for short) also known as (R)-( )-2-(hydroxymethyl)pyrrolidine ($C_5H_{11}NO$), is one such reagent. Chiral molecules with a hydroxyl functional group (AOH) that show hydrogen bonding effects are of structural and spectroscopic importance. The 2-PRDM has shown inter-molecular hydrogen bonding as seen in its vibrational IR spectrum. The hydrogen bonding has been a phenomenon of importance in the elucidation of molecular structure with wide ranging implications in chemical and biological studies. Despite having been defined and characterized over the years, the study of hydrogen bonding is revisited in the light of ab initio theoretical developments such as DFT thereby creating interest across disciplines [3]. In their study of vibrational circular dichroism (VCD) spectra of (R)-( )-2-butanol, Wang and Polavarapu have shown that, while the inter-molecular hydrogen bonding affects the conformational population of (R)-( )-2-butanol in solution phase in a negligible way, the same hydrogen bonding causes frequencies of CAOAH bending and CAO modes to increase [4]. Similarly, He and Polavarapu found that the agreement between theory and experi-ment for the determination of absolute configuration is satisfactory when the a-aryloxypropanoic acids (2-(2-chlorophenoxy) propa-noic and 2-(3-chlorophenoxy) propanoic acid) are converted to esters in solution phase thereby eliminating the dimerization due to hydrogen bonding effects [5]. Both these studies have demon-strated the need to understand and control the role of hydrogen bonding in conformational behavior, structural parameters and vibrational modes of the chiral molecules, (R)-( )-2-butanol, 2-(2-chlorophenoxy) propanoic and 2-(3-chlorophenoxy) propanoic acid. Other studies reported include vibrational assignments of Pyrrolidine and its deuterated derivatives and N-methylpyrrolidine-d_o by Billes and Geidel [6]. El-Gogary and Soliman reported similar assignments only for Pyrrolidine with envelop and twist conformers computed at MP2/6-31G′ [7].

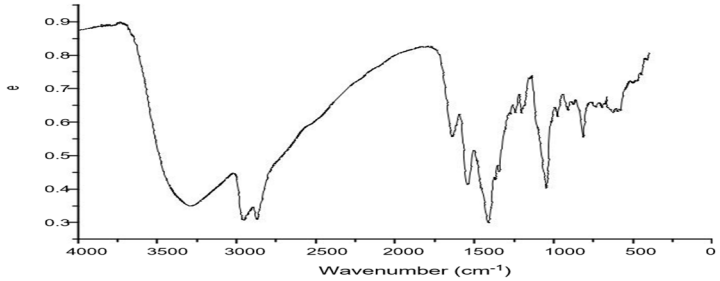

Fig. 2. Observed FT-IR spectrum of (R)-( )-2-Pyrrolidinemethanol.

ISSN: 2321-9653; IC Value: 45.98; SJ Impact Factor: 6.887
Volume 6 Issue XII, Dec 2018- Available at www.ijraset.com

In both these studies, the role of AOAH hydrogen bonding as well as its frequency shift in the neighbourhood of the NAH stretching band have not been considered. Morzyk-Ociepa et al., however, have reported a down-shifted NAH band at 3350 cm ^{1} distinctly away from OAH stretching band near 3052 cm ^{1} in the IR absorption spectrum of the solid Indole-2-carboxylic acid. These IR bands are attributed to NAH O and OAH O bindings and are supported by their XRD studies [8]. In the present paper we report an interpretation of the IR and Raman vibrational spectra of 2-PRDM aided by ab initio and DFT calculations of its conformers and dimeric species. The IR spectrum is marked by the presence of a broad down-shifted band structure near 3289 cm ^{1}. A series of concentration-dependent solution-phase IR spectra seem to suggest the absence of any intra-molecular hydrogen bonding. Based on this result, we have modelled two types of hydrogen bondings, namely, inter-molecular NAH O and OAH O bondings and have shown that the observed spectral features can be explained in terms of vibrational modes due to OAH O and NAH O bondings formed between pairs of monomer species (dimers) computed at B3LYP level combined with 6-311+G(d,p) basis set.

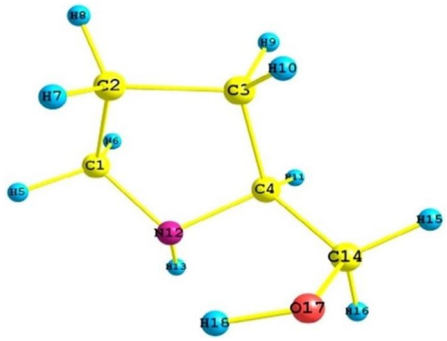

Fig. 1. Molecular structure of (R)-( )-2-Pyrrolidinemethanol.

II. EXPERIMENTAL

The liquid sample was purchased from Sigma–Aldrich and was used without further purification. The FT IR absorption spectra were measured on Nicolet's Impact 410 FTIR Spectrometer with a resolution of 1 cm ^{1}. The sample was smeared on KBr windows and was illuminated using ETC Ever-Glo™ midIR source in the spectrometer. The signals were collected by Deuterated Lanthanium Triglycine Sulfate detector (DLaTGS). In order to achieve good signal-to-noise ratio 100 scans were accumulated and averaged. The FT Raman spectral measurements were made on a Bruker Multi-Ram FT Raman spectrometer with the interfer-ometer bench comprising a CaF_2 beam splitter and an LN2 cooled Ge detector. A diode-pumped air-cooled cw Nd–YAG laser source provided excitation line at 1064 nm (93,985 cm ^{1}). The spectra were measured with a total of 100 scans at a resolution of 1 cm ^{1}. A series of IR absorption spectra of the sample in carbon tetra-chloride were measured in the concentration range 10.0– 1.0 10 ^{2} M, using the same spectrometer parameters as for the neat liquid sample.

III. COMPUTATIONAL

Ab initio and density functional theory (DFT) calculations were carried out using Gaussian 09W and GaussView 5.0 suite of programs [9,10]. The theoretical levels for the calculation include RHF combined with 3-21G and B3LYP combined with 6-311+G(d,p) basis sets. The B3LYP combination of functionals is known to predict vibrational frequencies and IR intensities fairly accurately for large ring molecules and this has been found to be true in the present study. In order to search for possible stable conformers, a relaxed potential energy surface (PES) scan at RHF/3-21G level was performed by varying dihedral angles NAC′ACAO and C′ACAOAH (where C′ refers to carbon atom at chiral center in the molecule $C_5H_{11}NO$) simultaneously from 0

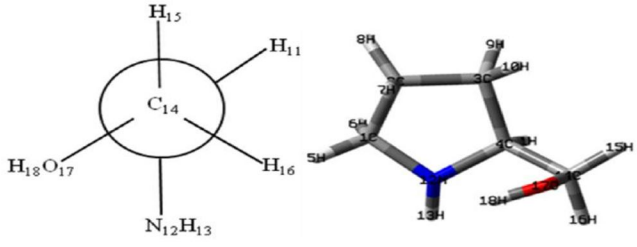

(a) G_{-1}: NCCO=−54˚

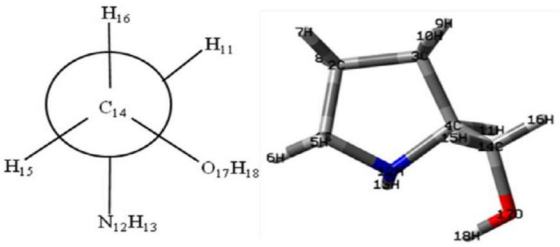

(b) G_{+1}: NCCO= 54˚

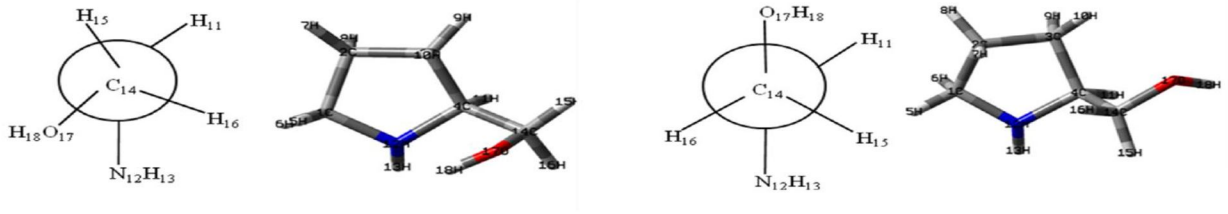

(c) G_{-2}: NCCO=−49˚ (d) T: NCCO=−175˚

Fig. 3. Conformers at B3LYP/6-311+G(d,p) of 2-PRDM using Newmann projections (viewed along $C_{14}AC_4$).

Table 1
Conformers and their relative Gibbs free (DG) energies, Boltzmann populations of conformers of (R)-( )-2-Pyrrolidinemethanol.

Conformers	Relative DG (kcal mol ^{1})	Population (%)
^{G} 1	0.0	38.7
^{G}+1	0.075	34.2
^{G} 2	0.282	24.1
T	2.271	1.9

Table 2 Optimized geometrical parameters of the conformers G $_1$, G$_{+1}$, G $_2$, T.

^{0}	Conformers				
Bond length (ÅA)					
	G 1	G +1	G 2	T	PY[a]
C1AC2	1.532	1.545	1.537	1.541	1.543
C1AH5	1.093	1.081	1.095	1.082	1.082
C1AH6	1.103	1.081	1.093	1.088	1.089
C1AN12	1.467	1.485	1.484	1.477	1.469
C4AN12	1.479	1.493	1.486	1.479	1.469
N12AH13	1.014	1.006	1.012	1.001	1.013
C14AO17	1.418	1.432	1.417	1.445	–
O17AH18	0.969	0.971	0.971	0.966	–
Bond angle (L)					
C2AC1AH5	113.2	110.4	110.4	112.5	–
C2AC1AH6	110.2	113. 5	112.9	109.6	–
C2AC1AN12	102.3	104.6	105.6	102.6	104.6
H5AC1AN12	110.7	109.0	109.6	110.9	–
H6AC1AN12	112.5	110.6	111.1	112.5	–
C1AC2AC3	103.6	103.2	102.5	102.5	104.9
C1AN12AC4	107.9	106.5	109.8	110.9	105.2
C3AC4AC14	114.5	112.6	114.7	111.0	104.9
C4AN12AH13	112.3	111.9	111.6	116.1	107.0
N12AC4AC14	108.9	106.9	109.3	108.1	104.6
C4AC14AH15	110.4	109.1	110.5	110.0	–
C4AC14AO17	111.4	109.5	111.3	111.6	–
C14AO17AH18	104.9	105.7	104.5	110.4	–
Torsional angle (L)					
N12AC4AC14AO17	54.79	54.22	48.74	174.46	–
C4AC14AO17AH18	43.29	46.05	44.34	69.52	–

Note: PY[a] = Pyrrolidine, experimental values from electron diffraction study [13].

Table 3a
Gibbs free energy (DG), relative energy and Boltzmann population of the inter-molecular OAH O bonded dimer species.

Dimer	Monomers	DG (hartree)	Relative energy difference (kcal/mol)	Relative population (%)
D_1	$^{G}1$ with G_{+1}	654.164224	0.00	66.9
D_2	$^{G}2$ with G_2	654.162852	0.86	15.7
D_3	$^{G}1$ with G_2	654.161304	0.97	13.1
$^{D}4$	$^{G}1$ with G_1	654.158669	1.65	04.1

Table 3b
Gibbs free energy (DG), relative energy and Boltzmann population of the inter-molecular NAH O bonded dimer species.

Dimer	Monomers	DG (hartree)	Relative energy difference (kcal/mol)	Relative population (%)
D_1	G_1 with G_{+1}	654.164521	0.00	28.3
$^{D}2$	$^{G}2$ with G_2	654.164489	0.02	27.3
D_3	$^{G}1$ with G_2	654.164156	0.23	19.2
D_4	$^{G}1$ with G_1	654.163985	0.34	16.1
D_5	G_{+1} with G_{+1}	654.163421	0.69	08.8

These conformers lay closer to their stationary points on the PES and therefore, we further optimized the four conformers by performing harmonic frequency analysis at B3LYP/6-311+G(d,p) level by taking the PES results at RHF/3-21G level as input. These steps saved computational cost. Since the IR spectrum of (R)-( )-2-Pyr rolidinemethanol has shown evidence of a hydrogen bonding, we modeled the hydrogen bonding by considering different intra-and inter-molecular dimer species with the four predicted mono-mers (conformers). The results are discussed in the later sections. Since the molecule is also chiral, its rotational strength values, R, defined as the scalar product of molecular electric and magnetic dipole transition moments were computed and plotted vs wave number of bands, giving simulated spectra[11].

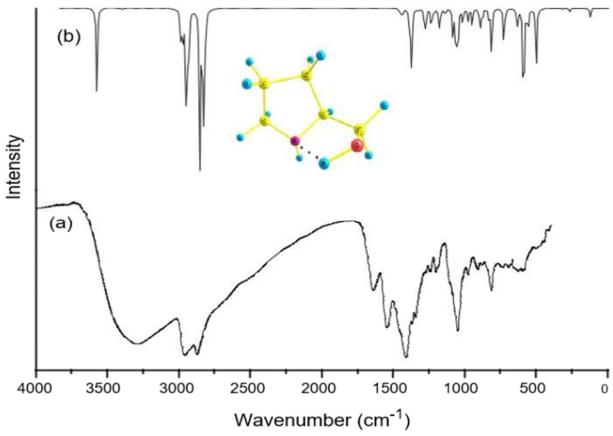

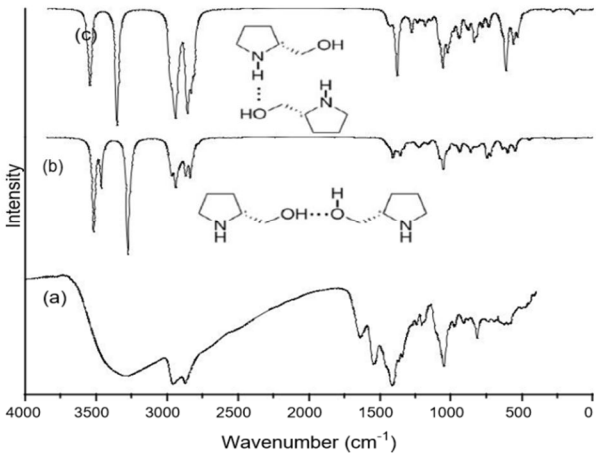

Fig. 4. Observed FT-IR (a) and simulated Boltzmann-weighted intra-molecular monomer (b) IR spectra and intra molecular OAH N bonded molecular structure of 2-PRDM Fig. 5. Observed FT-IR spectrum (a) and, simulated Boltzmann-weighted-dimer OAH O (b), dimer NAH O (c) FT-IR spectra of 2-PRDM.

IV. RESULTS AND DISCUSSION

A. *Conformational and Hydrogen Bond Analysis*

The molecular structure of 2-PRDM is shown in Fig. 1. The observed IR spectral features near 3290 cm ^{1} with fwhm 700 cm ^{1}, as shown in Fig. 2 (showing only experimental IR), strongly indicate that there exists some kind of intra- or inter-mo-lecular hydrogen bonding. For (R)-( )-2-butanol, Wang and Polavarapu have reported that the hydrogen bonding causes fre-quencies of CAOAH bending and CAO modes to increase. It follows that the vibrational structure of such chiral molecules is modified by the presence of the hydrogen bonding [4]. Therefore, we consid-ered intra-molecular hydrogen bonding, OAH N (for brevity, we call this type of bonding, Type I) and inter-molecular hydrogen bonding, OAH O or NAH O (we call Type II and Type III respec-tively) between conformational monomers of the 2-PRDM as pos-sible factors for the interpretation. As a first step in modeling these molecular interactions, we searched for possible conformers by performing a relaxed potential energy surface scan (PES) at RHF/3-21G level of theory by varying the dihedral angles NAC′ACAO and C′ACAOAH simultaneously from 0L to 360L at 10L per interval. We found four conformers on the PES. For better results we further optimized the four conformers by performing harmonic frequency analysis at B3LYP/6-311+G(d,p) level by tak-ing the PES results at RHF/3-21G level as input. Of the four con-formers, the first three conformers are gauche conformers which we label G_{1}, G_{2}, G_{+1} and the fourth one is trans conformer, T. All the four conformers in the Newmann projection are shown in Fig. 3(a–d). The relative Gibbs free energies (DG) and the Boltzmann populations of the conformers are presented in Table 1. The imino hydrogen lies at equatorial position with the ring and methanol group forming the gauche structure in the most stable conformer, G_{1}, (i.e. the dihedral angle N12AC′4AC14AO17 = 55L). This conformational state is the most populated at 39%. The second most stable closer conformer is G_{+1} with a population of 34%, being separated from G_{1} by 0.075 kcal/-mol. The third conformer, G_{2}, with a population of 24%, is sepa-rated at 0.282 kcal/mol; the fourth one is T with 2% population at the energy 2.271 kcal/mol. With very small energy difference, G_{1} and G_{+1} lie very close on the PES, but they are conformationally distinct. The closeness in energy between the two conformers is also seen in their comparable Boltzmann populations. In the Table 2 are presented the optimized geometrical parameters of all the four conformers calculated at B3LYP/6-311+G(d,p) level. The values are compared with the electron diffraction measure-ments for Pyrrolidine [12,13]. It is to be noted that the computed bond lengths deviate within 1% of the experimental values, whereas the bond angles deviate as much as by 4%, pointing to slightly distorted Pyrrolidine ringAfter obtaining the conformers, we computed vibration spectra of monomers with Type I bonding. Similarly, we computed spectra of dimers with Type II and III bonding between pairs of the all four conformers. Geometry optimization of each pair was performed followed by harmonic frequency analysis, exactly in the same

Table 4
Computed vibrational frequencies (cm ^{1}) of free monomers, intra-molecularly bonded monomers and inter-molecularly bonded dimers compared with experimen-tal values.

Frequencies at B3LYP/6-311+G(d,p)				
Monomer	Intra-molecular OAH N Monomer		Inter-molecular H-bonded dimer	
		OAH O	NAH O	Assignments
3576	–	3517	3551	OAH stretching (free)
	3576	3275 (3289)	3545	OAH stretching (bonded)
3399	–	3405,	3399	NAH stretching (free)

	3399	3380 –	3353	NAH stretching (bonded)
	1281	–	1395 (1412)	NAH in-plane bending (bonded)
1281	–	1285, 1244	1239	NAH in-plane bending (free)
	1373	1409 (1412)	1376 (1369)	OAH in-plane bending (bonded)
1373	–	1358 (1369)	1280	OAH in-plane bending (free)
815	–	938, 901 (908)	893	NAH out-of-plane bending (free)
	815	–	808 (815)	NAH out-of-plane bending (bonded)
	591	599 (597)	544 (597)	OAH out-of-plane bending (bonded)
591	–	570 (578)	519	OAH out-of-plane bending (free)

Note: numbers within the brackets are observed IR frequencies.

manner as was done for monomers, giving rise to dimers with both the Type II and III bondings. For the Type II, calculations yielded four dimer species D_i (i = 1, 2, 3, 4, Table 3a). The most stable dimer D_1 has the highest population with 67%. The remaining dimers are thinly populated as shown in Table 3a. Similarly for Type III, calcu-lations yielded five dimer species D_i (i = 1, 2, 3, 4, 5, Table 3b). In these calculations, while dimers D_1 and D_2 have nearly the same populations as for D_3 and D_4, the D_5 has just 8%. For a good agreement between theory and experiment, Boltzmann population-weighted spectra were plotted as shown in Fig. 4(a) and (b) and Fig. 5(a–c) where they are compared with the experimental IR spectrum. Both computed and experimental IR frequencies of some of the important bands are summarized in Table 4. We see that the stretching OAH and NAH frequencies at 3576 cm ^{1} and 3399 cm ^{1} computed for Type I bonding are the same as for free monomer species. These two bands are away from the band measured at 3289 cm ^{1}. To ascertain whether or not Type I hydrogen bonding exists we measured a series of concentration-dependent IR solution spectra in carbon tetrachlo-ride in the range of 10.0–1.0 10 ^{2} M and the resultant spectra are presented in Fig. 6. A noticeable feature in the spectra is that the prominent band peaking at 3289 cm ^{1} shifts to 3450 cm ^{1} with diminishing intensity [14]. This observation is contrary to the nature of intra-molecular hydrogen bonding since such bond-ing is generally strong and does not, as a rule, shift frequency posi-tion [15]. Further, the bands due to free OAH and NAH have also not appeared [16]. Further, we note the gradual disappearance of almost all the bands beyond 0.1 M concentration except the broad band surviving as weak 'hump' near 3450 cm ^{1}. We offer no easy interpretation of these results. The band at 3450 cm ^{1} may be cor-related to the predicted monomer band at 3576 cm ^{1}. We were led, therefore, to the other two possibilities that the band at 3450 cm ^{1} is either due to Type II or Type III bonding. For the Type II bonding (see Table 4), a predicted band at 3517 cm ^{1} due to free OAH may correspond to the band at 3450 cm ^{1}; another predicted band at 3275 cm ^{1} due to bonded OAH is identified as the observed band at 3289 cm ^{1}. For the Type III, two predicted bands, one for free and one for bonded NAH are 3399 cm ^{1} and 3353 cm ^{1} respectively. As for the bands due to bending modes, bonded OAH frequency is 1409 cm ^{1} as against measured value of 1412 cm ^{1}. The monomer value is 1373 cm ^{1} and the magni-tude of this frequency is increased to 1409 cm ^{1} as is true in Type II bonding. In the case of Type III dimer calculations, the free NAH in-plane bending frequency is 1281 cm ^{1} as against a com-puted band at 1395 cm ^{1} in Type I. While the agreement between theory and experiment is excellent for both Type II and III

Table 6
Computed vibrational frequencies of monomer and OAH O dimer with experimen-tal IR and Raman frequencies and assignments for 2-PRDM.

Computed frequencies		Observed Frequencies		Assignment
Monomer Freq	Dimer Freq	IR (cm^{1})	Raman (cm^{1})	
3576	3517			OH stretching (79)
	3405			NH stretching (60)
3399	3380			NH stretching (63)
	3275	3289 vs Br		OH stretching (bonded) (72)
2986	2990			CH_2 asym stretching (63)
	2972			CH_2 asym stretching (68)
2970	2964			CH_2 asym stretching (63)
2951	2958	2957 vs	2959 vs	CH_2 asym stretching (63)
2948	2940		2940 sh	CH asym stretching (51)
2937	2921			CH_2 sym stretching (51)
2931	2904			CH_2 sym stretching (60)
	2870	2869 vs	2873 vs	CH_2 sym stretching (66)
2854	2862			CH_2 sym stretching (58)
2834	2836			CH stretching (61)
2824	2832			CH stretching (54)
1463	1459			CH_2 scissoring (68)
1452	1456		1452 ms	CH_2 scissoring (72)
1446	1445			CH_2 scissoring (73)
1431	1434			CH_2 scissoring (70)
1387	1409	1412 vs	1415 vw Sh	OH bend (66) + CH_2 scissoring (15)
1373	1358	1369 w Sh		OH bend (45) + CH_2 wag (25)
1336	1336	1342 sh	1348 sh	CH bend (84)
1327	1305		1315 vw Sh	CH bend (80)
1288	1301			CH_2 wag (85)
1281	1285			CH_2 wag (76) + NH in-plane wag (16)
1271	1275	1272 vw Sh	1274 w sh	CH_2 wag (79)
1236	1244	1241 Mw	1241 mw	CH + NH in-plane bend (out of phase) (78)
1216	1203	1204 Mw	1203 w	CH_2 twist (64)
1183	1174	1182 vw Sh		CH_2 twist (methanol) (68)
1171	1160			CH_2 twist (65)
1139	1156	1148 vw	1145 vw	CH_2 twist (68)
1085	1083	1096 vw Sh	1115 w	CH_2 rock (32) + ring asym stretching (46)
1064	1073			CH_2 rock (38) + ring asym stretching (42)
1052	1046	1047 s	1047 mw	CN stretching (38) + ring asym stretching (32)
1016	1010		1011 w	CO stretching (31) + ring asym stretching (48)
979	975	976 mw	982 vw	CACAC asym stretching (66)
950	938			NH out-of-plane bend (58)
896	901	908 mw	914 ms	OH out-of-plane bend (52)
889	891			Ring breathing (75)
878	875	873 vw	874 mw	Ring breathing (72)

834	825		820 mw Sh	Ring deformation (64) + CH_2 rock (18)
815	806	815 ms	804 mw	NH out-of-plane wag (58) + CH_2 rock (13)
728	745	732 vw		NH out-of-plane bend (71)
634	637	623 vw		Ring deformation (59)
	599	597 vw		OH out-of-plane deformation (bonded) (76)
561	570	578 vw		OH out-of-plane deformation (free) (47)
501	445	497vw	498w	CO torsion (45) + ring bend (puckered) (28)
	383			CACAC bend (59)
319	320			Ring-methanol torsion (49)

Note: *Frequencies (in cm ^{1}) are scaled with the factor 0.9613 [22] and Boltzmann population weighted, br = broad, sh = shoulder, s = strong, vs = very strong, ms = medium strong, w = weak, vw = very weak, mw = medium weak, sym = sym-metric, asym = asymmetric.

Bondings, the Type II modeling has produced results closer to experimental than the Type III. Finally, we look at the computed geometrical parameters for the Type I, II and III bondings as shown in Table 5. We see that, for both Type II and III bondings, the angle between XAH and H Y is near 172–176L suggesting a stronger bonding. The H Y distance, 1.852 Å, is shorter for Type II than the distance, 2.122 Å, for Type III bonding. It may be said that it is the Type II over Type III that meets both spectral and geometrical criteria satisfactorily [17]. If this is provisional conclusion, we allow for the possibility of both Type II and III bondings being pre-sent in the sample of 2-PRDM as is true of Indole-2-carboxylic acid reported by Morzyk-Ociepa et al. [7]. For Indole-2-carboxylic acid, a strong IR band at 3350 cm ^{1} is assigned to NAH stretching mode associated with Type III bonding and a satellite band at 3453 cm ^{1} being assigned to free NAH stretching mode. A strongly broad IR band near 3052 cm ^{1} is assigned to OAH stretching mode associ-ated with Type II bonding. The presence of these Type II and III bondings is directly confirmed by Morzyk-Ociepa et al. through X-ray diffraction study, showing both the OAH and NAH groups as donors and the oxygen, O, of the carboxylic moiety as acceptor. The computed hydrogen bonding parameters in the present study as shown in Table 5 compare fairly with the X-ray study values for Indole-2-carboxylic acid. The crystalline structure of Indole-2-carboxylic acid, among others, is a zig-zag pattern with sharp IR bands. In contrast, however, the 2-PRDM is a liquid sam-ple with its IR and Raman spectra being characterized by broad peaks in the region 2000–400 cm ^{1} demonstrating dominant inter-molecular Type II and III bondings. Raman bands near 980– 900 cm ^{1} are medium to strong modes in Pyrrolidine whereas they are weak in 2-PRDM, suggesting either large distortion to the ring or the ring is unable to vibrate due to strong Type II and III bondings.

V. VIBRATIONAL ANALYSIS

All the assignments of the measured IR and Raman bands are summarized in Table 6. The bands related to the Type II and III bondings are already assigned in Table 5. In both the spectra, bands due to methylene moieties show very well near 2990–1200 cm From the spectra-structure correlations view-point, it would be of value if we compared all the modes of 2-PRDM with those of Pyrrolidine as assigned by others and they are presented in Table 7.

A. CH Vibrations

The CH_2 modes are characteristically Raman strong and there-fore have dominated the Raman spectrum (Fig. 7). This also true of the IR spectrum but it has modes originating mostly from NAH vibrations. The methylene stretching modes appear in the region 2970–2940 cm ^{1} [18,19]. In the parent Pyrrolidine molecule (PY) [6,7] the same modes are observed in the region 2970– 2820 cm ^{1}. Two CH_2 groups in the ring stretching asymmetrically in phase with each other is assigned to strong bands at 2957 and 2959 cm ^{1} in the IR and Raman spectra respectively. The same mode is computed at 2958 cm ^{1}. In another mode where again the same groups are asymmetrically stretching but are out of phase with each other is assigned to 2940 cm ^{1} in the Raman. The ring CH_2 symmetric stretching mode appears very strongly at 2869 cm ^{1} and 2873 cm ^{1} as IR and Raman bands respectively. Since the molecular monomers exists as different bonded dimer species, the number of CH_2 and CH bands is doubled, although not all of them are observed but their frequency values are com-puted. Two CH_2 groups are scissoring out of phase with each other and their computed mode is 1456 cm ^{1}; it appears as a medium strong Raman mode at 1452 cm ^{1}. Another CH_2 scissoring mode computed at 1409 cm ^{1} is a coupled mode with OAH bend; it appears as very strong IR mode at 1412 cm ^{1} while it is a weak

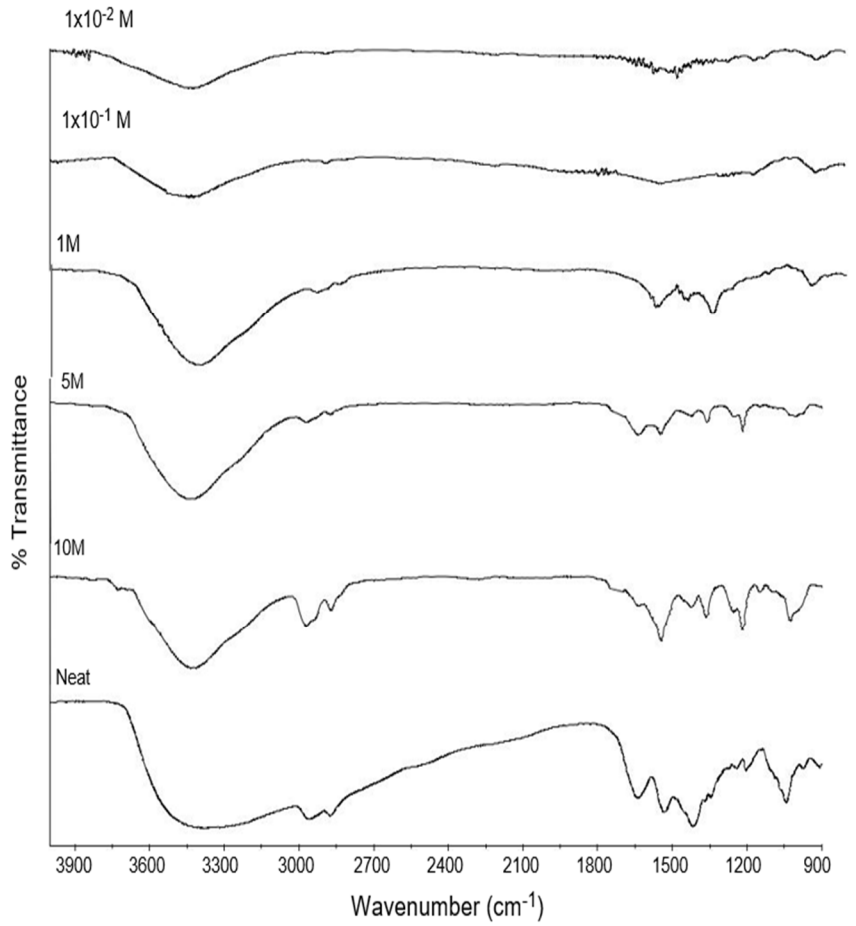

Fig. 6. IR spectra of 2-PRDM as a function of different concentrations in CCl_4 solvent.

Table 5
Computed intra- and inter-molecular hydrogen bonding geometrical parameters of 2-PRDM.

XAH Y	Intra-molecular OAH N monomer	Inter-molecular OAH O dimer	Inter-molecular NAH O dimer
XAH (Å)	0.969	0.974	1.017
H Y (Å)	2.265	1.852	2.122
X Y (Å)	3.234	2.826	3.139
\XAH Y (L)	114	172	176
H-bonded structures	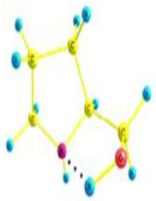	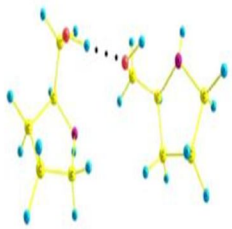	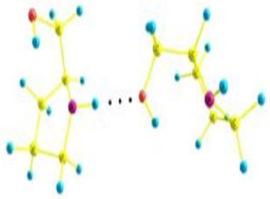

Raman shoulder at 1415 cm ^{1}. The CH_2 wagging mode is very weak in both IR and Raman at 1272 cm ^{1}, while the twisting modes of medium weak intensity appear at 1204 cm ^{1}.

Table 7 Comparison of assignments of Pyrrolidine by different workers with those for 2-PRDM.

Ref: Billes	Ref: El-Gogary		Present work			Assignment
IR	IR	Raman	IR	Raman	DFT-dimer	
					3517	OH stretch (free)
3356		3355 vw, p			3380	NH stretch
		3310 vw, p				–
	3264 vs	3270 w, sh				NH stretch
			3289 vs br		3275	OH stretch (bonded)
2967					2964	CH stretch
	2957 vs	2960 vs p	2957vs	2959 vs	2958	CH_2 asym stretch
2927					2921	CH stretch
2916	2910 s, sh	2910 s, sh			2904	CH stretch
2889						CH stretch
2879		2876 vs	2869 vs	2873 vs	2870	CH_2 sym stretch
	2866 s				2862	CH stretch
2824					2832	CH stretch
2818	2818 m	2818 m				CH stretch
1484	1486w, sh	1485s sh				CH_2 scissor
1459	1458 s	1460 s sh			1459	CH_2 scissoring
1447	1451 m sh	1450 vs	–	1452 ms	1456	CH_2 scissoring
1412	1415 m	1412 w sh	1412 vs	1415 vw, sh	1409	OH bend + CH_2 scissoring
	1400 m sh					Sym CH_2 wag
		1354 vw	1369 w sh		1358	OH bend + CH_2 wag
1341	1337 w	1340 vw	1342 sh	1348 sh	1336	CH, NH deformation
1292	1300 w sh			1315 vw sh	1305	HNC wag
1273	1285 m	1285 w, p	1272 vw sh	1274 w sh	1275	CH deformation
1268						CH deformation
						CH + NH in-plane bend (out of
1228			1241 mw	1241 mw	1244	phase)
1211		1220 m, p				CH deformation
1203			1204 mw	1203 w	1203	CH_2 twist
1181	1195 m	1197 w, sh	1182 vw sh		1174	CH_2 twist
			1148 vw	1145 vw	1156	CH_2 twist
1099	1108 vw sh	1106 vw	1096 vw sh	1115 w	1083	Ring asym stretch + CH_2 rock
1023	1023 w sh	1025 s, p	1047 s	1047 mw	1046	CN stretch + ring asym stretch
			–	1011 w	1010	CO stretch + ring asym stretch
974	980 m	975 s	976 mw	982 vw	975	CACAC asym stretch
920	915 s	915 m, p			938	NH out-of-plane bend
			908	914	901	OH out-of-plane bend
871	870 vs		873 vw	874 mw	875	CACAC sym stretch
				820 mw sh	825	Ring deformation + CH_2 rock
	800 vs sh	800 vw, p	815 ms	804 mw	806	NH out-of-plane wag + CH_2 rock
789	770 vw sh	778 vw				CH_2 rock
			732 vw		745	NH out-of-plane bend
600	605 w	605 w	623 vw		637	Ring def
			597 vw		599	OH out-of-plane def (bonded)
			578 vw		570	OH out-of-plane def (free)
			497 vw	498 w	445	CO torsion + ring bend
					383	CACAC bend
					320	Ring-methanol torsion

Note: all frequencies in cm^{-1}, dimer frequencies are those of computed dimer OAH O model, br = broad, sh = shoulder, s = strong, vs = very strong, ms = medium strong, w = weak, vw = very weak, mw = medium weak, sym = symmetric, asym = asymmetric.

B. CN Vibrations

CAN stretching mode is strong in the IR as compared to its Raman mode at 1047 cm^{-1}. The calculated value at 1046 cm^{-1} is also in agreement with the observed mode.

C. The OH and NH Vibrations

A strong and broad absorption band at 3289 cm ^{1} is not only region of NAH stretching vibration but possibly the region of down-shifted OAH stretching vibration [20]. However, as we have analysed the region in the preceding section, the region near 3289 cm ^{1} is identified as the bonded OAH stretching vibration masking the free NAH stretching vibration, and therefore, we assign the 3289 cm ^{1} band to the OAH stretching mode. The com-puted value is at 3275 cm ^{1}. And the non-bonded OAH stretching mode is computed at 3517 cm ^{1}. The predicted NAH stretching modes in the dimer are at 3405 cm ^{1} and 3380 cm ^{1}. Our solvent spectra have shown that the 3289 cm ^{1} shifts to the region 3450– 3430 cm ^{1} and remains constant in the position but only diminish-ing in the intensity at lower concentrations; the bonded OAH stretching mode still completely masks the expected NAH mode. The OAH in-plane deformation mode is a very strong IR mode at 1412 cm ^{1} but its counterpart in Raman is a weak shoulder at 1415 cm ^{1}. The out-of-plane deformation modes of the bonded and free OAH predicted at 599 cm ^{1} and 570 cm ^{1} respectively, are very weak IR bands observed at 597 cm ^{1} and 578 cm ^{1} because the region is masked by the presence of broad and diffuse bands. The region 600–400 cm ^{1} is characterized by diffuse bands [21]. The NAH coupled with CAH in-plane deformation mode is observed at 1241 cm ^{1} in both IR and Raman and is computed at 1244 cm ^{1}. The NAH out-of-plane deformation mode is computed at 938 cm ^{1} while the same mode is assigned to 920 cm ^{1} [6] and to 915 cm ^{1} in Pyrrolidine [7]. Two additional modes are observed at 1636 cm ^{1} (overtone of 815 cm ^{1}) and 1545 cm ^{1} (combination of 815 cm ^{1} and 732 cm ^{1}

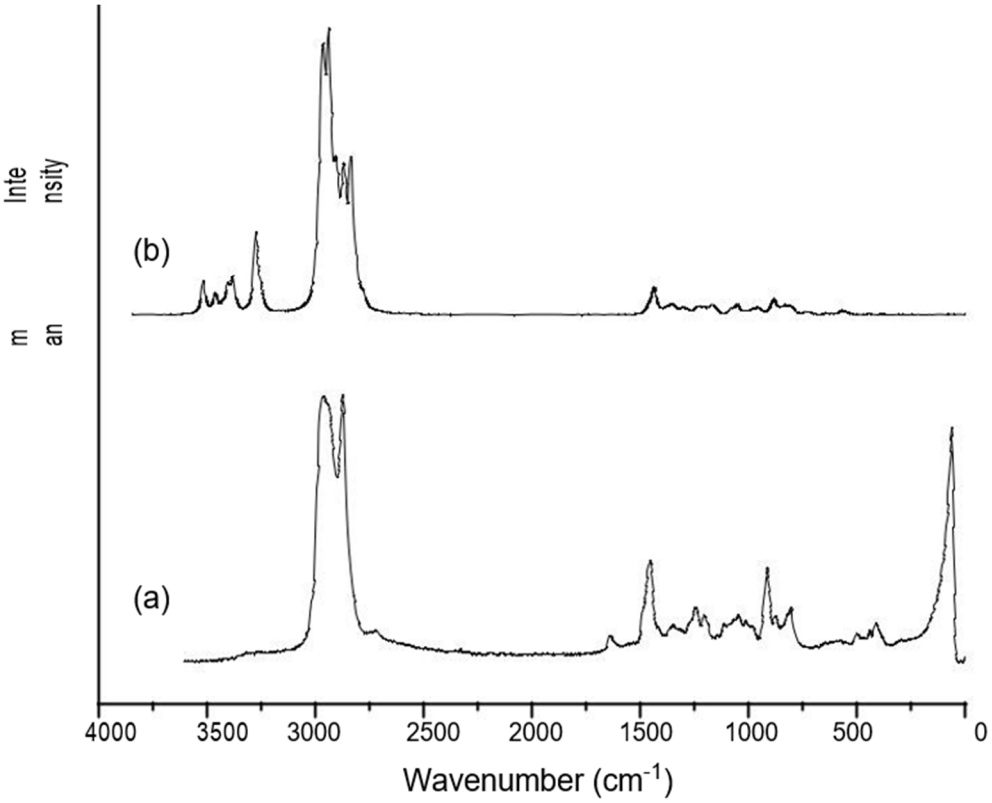

Fig. 7. Observed (a) and simulated Boltzmann-weighted dimer (b) Raman spectra of 2-PRDM.

D. CO Vibrations

A weak Raman mode at 1011 cm ^{1}, assigned to CO stretching vibration, is not observed in IR, but predicted at 1010 cm ^{1}. The CO torsional mode is assigned to 497 cm ^{1} in both IR and Raman and is predicted at 445 cm ^{1}.

E. Ring Vibrations

While the ring breathing vibration computed at 875 cm ^{1} and is assigned to an IR band at 873 cm ^{1} and Raman band 874 cm ^{1}, the asymmetric breathing mode computed at 891 cm ^{1} is not observed in both the spectra. Ring deformation mode is very weak as IR band at 623 cm ^{1}, while corresponding Raman band is not observed. In the parent Pyrrolidine, the mode is observed at 605 cm ^{1}. The ring bend (puckering) is assigned to a very weak IR band at 497 cm ^{1} and the ring torsional mode is computed at 323 cm ^{1} .

F. Computed VCD Spectrum

Since 2-PRDM is a chiral molecule, we have computed, for the sake of completeness, its rotational strength, R values for all the

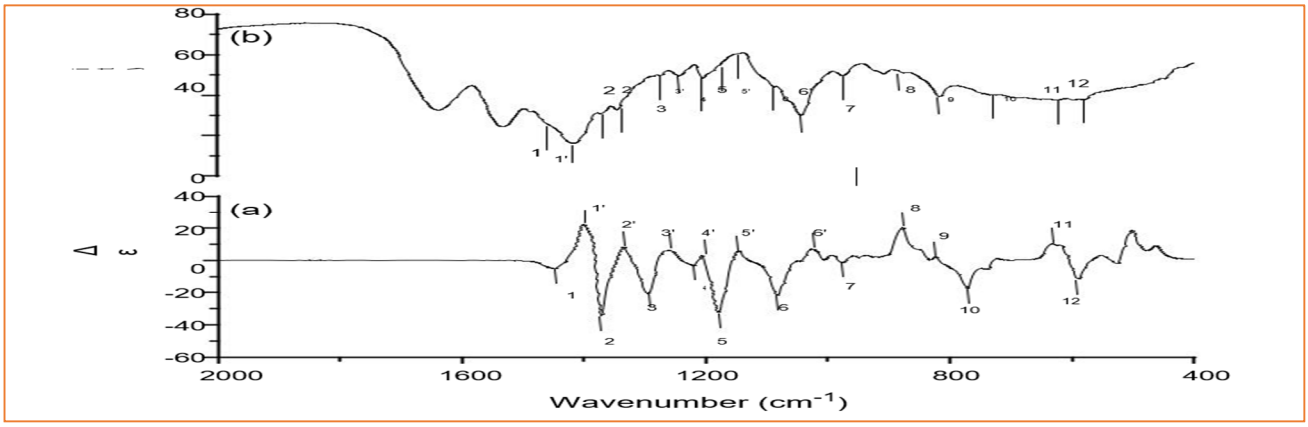

Fig. 8. Simulated Boltzmann-weighted monomer VCD spectra (a) and observed IR (b) in the region 2000–400 cm [1].

Table 8

Correlation of experimental IR frequencies with computed VCD bands with assignment.

Band No.	Experimental IR Freq (cm [1])	Predicted VCD band positions (cm [1])	Assignment
1	1439	1446	CH_2 scissoring
1^0	1412	1402	OH bend + CH_2 scissoring
2	1369	1373	OH bend + CH_2 wag
$_2 0$	1342	1337	CH bend
3	1272	1294	CH_2wag
3^0	1241	1259	CH + NH in-plane bend (out of phase)
4	–	1225	CH_2 twist
4^0	1204	1205	CH_2 twist
5	1182	1178	CH_2 twist (methanol)
5^0	1148	1146	CH_2 twist
6	1096	1085	CH_2 rock + ring asym stretching
6^0	1047	1025	CN str + ring asym stretching
7	976	972	CACAC asym stretching
8	873	877	Ring breathing
9	815	822	NH out-of-plane wag
10	732	773	NH out-of-plane bend
11	623	628	Ring deformation
12	578	586	OH out-of-plane deformation

Conformers and a Boltzmann weighted-VCD spectrum is simulated conformers and a Boltzmann weighted-VCD spectrum is simulated for the region 2000–400 cm ^{1} (this is the region where an experimental VCD spectrum strongly correlates to chiral structure) Correlation between IR and VCD bands is facilitated by the presence of coupled modes of both linear and oscillatory vibrations in this spectral region. It is apparent from the Fig. 8 that the weak or shoulder IR bands correspond to resolved negative or positive bands (bisignate couplets, [23]). Table 8 gives the following assignments. The bisignate couplet 1 and 1^0 are assigned to CH_2 scissoring and OAH coupled with CH_2 scissoring modes respectively. The bands 2 and 2^0 relate to OAH and CAH bend respectively. The absorption band 1 is a shoulder to band 1^0. Similarly 2^0 being a shoulder to 2 in the absorption spectrum, the corresponding VCD intensity of 1^0 and 2 is more than that of 1 and 2^0. A series of modes due to CH_2 deformation are assigned to 3, 3^0; 4, 4^0 and 5, 5^0. The couplet 6, 6^0 refers to ring asymmetric stretching modes. A band at 12 is due to OAH out-of-plane deformation.

VI. CONCLUSIONS

Vibrational modes of dimers of (R)-( )-2-Pyrrolidinemethanol due to intermolecular bonding NAH O and OAH O, at B3LYP/6-311+G(d,p) level are in good agreement with suggests that the OAH O is a stronger bond. We conclude that all the results point to the presence of both types of hydrogen bonds. However, it has not been possible us certain either by the solution phase IR spectra or by dimer calculations as to which time a bonding is the determinant factor for the observed spectral features. Perhaps calculations beyond dimerization such as trimerization or even beyond might be necessary to satisfactorily characterize these hydrogens bonds along with some more detailed solution phase IR measurements .

REFERENCES

[1] W.H. Brooks, W.C. Guida, K.G. Daniel, Curr. Top. Med. Chem. 11 (7) (2011) 760– 770.
[2] <www.sigmaaldrich.com>.
[3] F. Weinhold, R.A. Klein, Mol. Phys. 110 (9–10) (2012) 565–579.
[4] F. Wang, P.L. Polavarapu, J. Phys. Chem. A 104 (2000) 10683–10687.
[5] J. He, P.L. Polavarapu, Spectrochim. Acta A 61 (2005) 1327–1334.
[6] F. Billes, E. Geidel, Spectrochim. Acta A 53 (1997) 2537–2551.
[7] T.M. El-Gogary, M.S. Soliman, Spectrochim. Acta A 57 (2001) 2647–2657.
[8] B.M. Ociepa, D. Michalska, A. Pietraszko, J. Mol. Struct. 688 (2004) 79–86.
[9] M.J. Frisch, G.W. Trucks, H.B. Schlegel, G.E. Scuseria, M.A. Robb, J.R. Cheeseman, G. Scalmani, V. Barone, B. Mennucci, G.A. Petersson, H. Nakatsuji, M. Caricato, X. Li, H.P. Hratchian, A.F. Izmaylov, J. Bloino, G. Zheng, J.L. Sonnenberg, M. Hada, M. Ehara, K. Toyota, R. Fukuda, J. Hasegawa, M. Ishida, T. Nakajima, Y. Honda, O. Kitao, H. Nakai, T. Vreven Jr., J.A. Montgomery, J.E. Peralta, F. Ogliaro, M. Bearpark, J.J. Heyd, E. Brothers, K.N. Kudin, V.N. Staroverov, R. Kobayashi, J. Normand, K. Raghavachari, A. Rendell, J.C. Burant, S.S. Iyengar, J. Tomasi, M. Cossi, N. Rega, J.M. Millam, M. Klene, J.E. Knox, J.B. Cross, V. Bakken, C. Adamo, J. Jaramillo, R. Gomperts, R.E. Stratmann, O. Yazyev, A.J. Austin, R. Cammi, C. Pomelli, J.W. Ochterski, R.L. Martin, K. Morokuma, V.G. Zakrzewski, G.A. Voth,
P. Salvador, J.J. Dannenberg, S. Dapprich, A.D. Daniels, Ö. Farkas, J.B. Foresman, J.V. Ortiz, J. Cioslowski, D.J. Fox, Gaussian 09, Revision A.1, Gaussian Inc., Wallingford CT, 2009.
[10] R. Dennington, T. Keith, J. Millam, GaussView 5.0, Semichem Inc., 2009.
[11] L.A. Nafie, Vibrational Optical Activity: Principles and Applications, John Wiley & Sons Ltd., Chichester, 2011.
[12] G. Pfaferott, H. Oberhammer, J.E. Boggs, W. Caminati, J. Am. Chem. Soc. 107 (1985) 2305–2309.
[13] G. Pfaferott, H. Oberhammer, J.E. Boggs, J. Am. Chem. Soc. 107 (1985) 2309– 2313.

[14] C.N.R. Rao, Chemical Applications of Infrared Spectroscopy, Academic Press, New York and London, 1963.
[15] M. Davies, Infrared Spectroscopy and Molecular Structure, Elsevier Publication Company, Amsterdam, 1963.
[16] P. Schuster, G. Zundel, C. Sandorfy, The Hydrogen Bond: Recent Developments in Theory and Experiments II Structure and Spectroscopy, North-Holland Publishing Company, Amsterdam, New York, Oxford, 1976.
[17] E. Arunan, G.R. Desiraju, et al., Pure Appl. Chem. 83 (8) (2011) 1637–1641.
[18] G. Socrates, Infrared Characteristic Group Frequencies, John Wiley, GB, 1980.
[19] N.B. Colthup, L.H. Daly, S.E. Wiberley, Introduction to Infrared and Raman Spectroscopy, Academic Press Inc., New York, 1964.
[20] G. Desiraju, T. Steiner, The Weak Hydrogen Bond, in Structural Chemistry and Biology, Oxford Univ. Press Inc., New York, 2001
[21] T.S. Perova, D.H. Christensen, U. Rasmussen, J.K. Vij, O.F. Nelson, Vib. Spectrosc. 18 (1998) 149–156.
[22] A.P. Scott, L. Random, J. Phys. Chem. 100 (1996) 16502–16513.
[23] P.L. Polavarapu, C. Zhao, Fresenius J. Anal. Chem. 366 (2000) 727–734

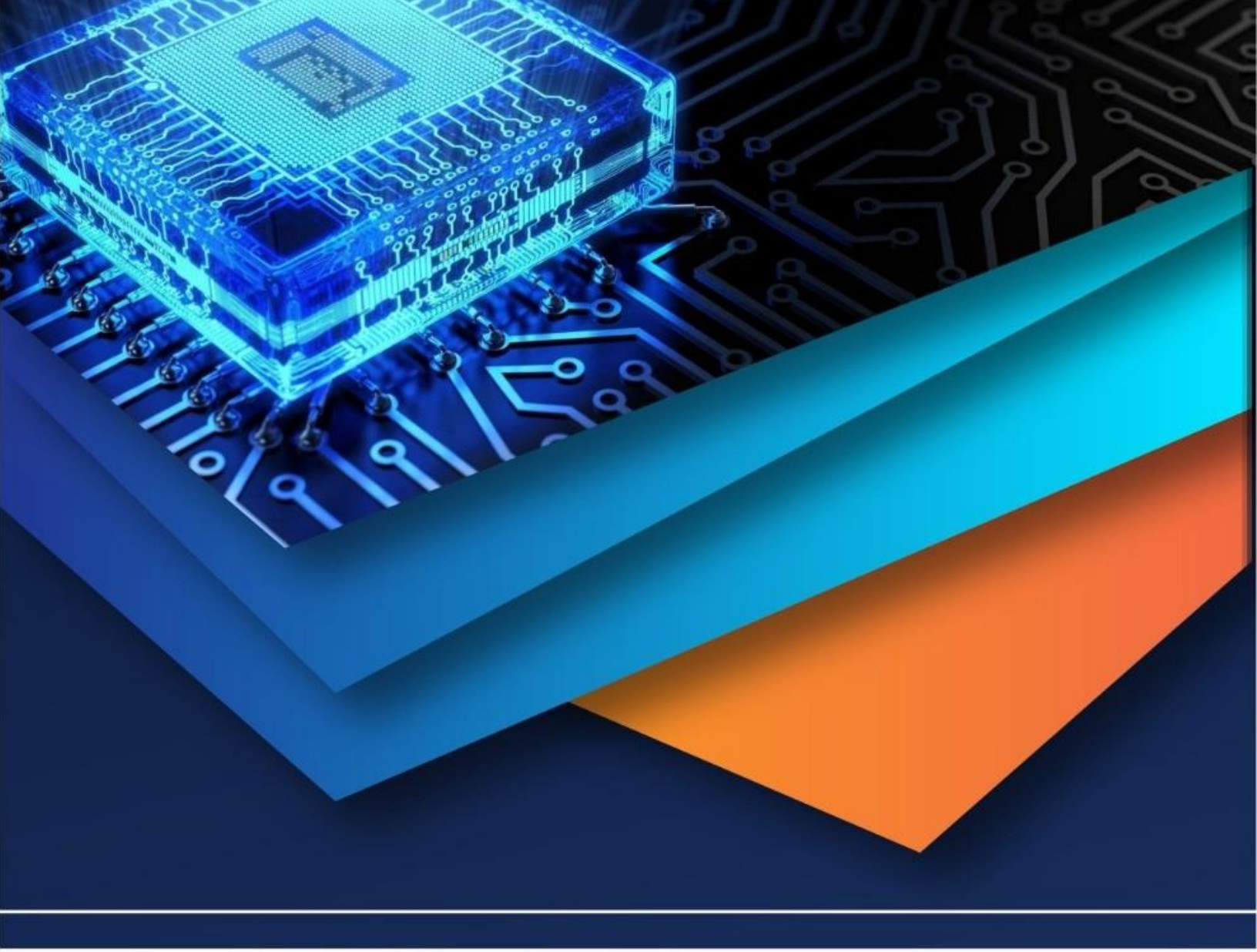

10.22214/IJRASET

45.98

IMPACT FACTOR: 7.129

IMPACT FACTOR: 7.429

INTERNATIONAL JOURNAL FOR RESEARCH

IN APPLIED SCIENCE & ENGINEERING TECHNOLOGY